



# Stalagmite-inferred European westerly drift in the early Weichselian with centennial-scale variability in marine isotope stage 5a

Yun-Chuan Chung<sup>a, b, c</sup>, Laurie Menviel<sup>d</sup>, Arianna Marchionne<sup>e</sup>, Horng-Sheng Mii<sup>f</sup>,  
Véronique Michel<sup>g, h</sup>, Patricia Valensi<sup>i, j</sup>, Xiuyang Jiang<sup>k</sup>, Patrick Simon<sup>l</sup>,  
Elena Rossoni-Notter<sup>l</sup>, Abdelkader Moussous<sup>l</sup>, Heikki Seppä<sup>c</sup>, Yu-Tang Chien<sup>m</sup>,  
Chung-Che Wu<sup>n</sup>, Hsun-Ming Hu<sup>a, b, \*\*</sup>, Chuan-Chou Shen<sup>a, b, \*</sup>

<sup>a</sup> High-Precision Mass Spectrometry and Environment Change Laboratory (HISPEC), Department of Geosciences, National Taiwan University, Taipei, 10617, Taiwan, ROC

<sup>b</sup> Research Center for Future Earth, National Taiwan University, Taipei, 10617, Taiwan, ROC

<sup>c</sup> Department of Geosciences and Geography, University of Helsinki, Finland

<sup>d</sup> Climate Change Research Centre, School of Biological, Earth and Environmental Sciences, UNSW Sydney, Sydney, New South Wales, Australia

<sup>e</sup> Department of Mathematics and Statistics, University of Helsinki, Finland

<sup>f</sup> Department of Earth Sciences, National Taiwan Normal University, Taipei, 11677, Taiwan, ROC

<sup>g</sup> Université Côte d'Azur, CNRS, CEPAM, 06300, Nice, France

<sup>h</sup> Université Côte d'Azur, CNRS, Observatoire de la Côte d'Azur, IRD, Géoazur, 06560, Valbonne, France

<sup>i</sup> HNHP (MNHN-CNRS-UPVD), Département Homme et Environnement, MNHN, 75013, Paris, France

<sup>j</sup> Musée de Préhistoire, 06690, Tourrette-Levens, France

<sup>k</sup> Key Laboratory of Humid Subtropical Eco-Geographical Processes, Ministry of Education, College of Geography Science, Fujian Normal University, Fuzhou, 350117, China

<sup>l</sup> Musée d'Anthropologie préhistorique de Monaco, 98000, Monaco, Monaco

<sup>m</sup> National Science and Technology Center for Disaster Reduction, New Taipei City, 23143, Taiwan, ROC

<sup>n</sup> Laboratory of Inorganic Chemistry, Department of Chemistry and Applied Biosciences, ETH Zurich, 8093, Zurich, Switzerland

## ARTICLE INFO

### Article history:

Received 13 October 2021

Received in revised form

22 May 2022

Accepted 22 May 2022

Available online 3 June 2022

Handling Editor: Mira Matthews

### Keywords:

Southern Europe

Stalagmite

Model simulation

Precipitation

Weichselian

MIS 5a

Multi-centennial arid intervals

AMOC

## ABSTRACT

The Weichselian glaciation is characterized by significant ocean circulation variations starting from ~115 thousand years ago (ka) and terminating at ~11.5 ka. The early Weichselian (115–74 ka), especially marine isotope stage (MIS) 5a at 85–74 ka, provides a window for understanding the linkage between the European westerlies and Mediterranean climate. However, lack of highly-resolved paleoclimate records with absolute chronologies hampers our knowledge of decadal-to-centennial-scale climate changes and forcings in the circum-Mediterranean realm. Here, we present <sup>230</sup>Th-dated stalagmite-inferred hydroclimate records from Observatoire cave (43°44' N, 7°25' E), Monaco, for the period between 88.7 ± 0.4 and 80.3 ± 0.1 ka, covering portions of MIS 5b and 5a. Agreement between Observatoire and circum-Mediterranean stalagmite records confirm large-scale warming over the Atlantic-Europe territory during the transition from MIS 5b to 5a. Subdecadally-resolved Observatoire δ<sup>18</sup>O and δ<sup>13</sup>C records express four multi-centennial arid intervals in southern Europe at 84–80 ka in the first-half of MIS 5a, suggesting centennial westerly drifts, a finding supported by a model simulation. Westerly changes and associated arid events can be attributed to slowdowns of the Atlantic meridional overturning circulation, North Atlantic Oscillation states, and solar activity.

© 2022 Elsevier Ltd. All rights reserved.

\* Corresponding author. High-Precision Mass Spectrometry and Environment Change Laboratory (HISPEC), Department of Geosciences, National Taiwan University, Taipei, 10617, Taiwan, ROC.

\*\* Corresponding author. High-Precision Mass Spectrometry and Environment Change Laboratory (HISPEC), Department of Geosciences, National Taiwan University, Taipei, 10617, Taiwan, ROC.

E-mail addresses: [hsunming.hu@gmail.com](mailto:hsunming.hu@gmail.com) (H.-M. Hu), [river@ntu.edu.tw](mailto:river@ntu.edu.tw) (C.-C. Shen).

## 1. Introduction

The last glacial cycle, starting from marine isotope stage (MIS) 5e at ~130 thousand years ago (ka, relative to AD 1950; hereafter), features rapid and recurrent millennial climate variations, as documented in Greenland ice cores with relatively warm

interstadials (GI) and cold stadials (GS) (Johnsen et al., 1992; Dansgaard et al., 1993; NorthGRIP-Members, 2004) (Fig. 1a). Northern hemisphere summer insolation (NHSI) peaks (Fig. 1b) brought warm temperatures and ice volume reductions, interrupting the Earth's transition from the last interglacial to last glacial maximum (Lambeck and Chappell, 2001). In the early Weichselian (~115–74 ka), two warm intervals, MIS 5c and 5a (Fig. 1) started following the NHSI maximum at 105 and 85 ka (Fig. 1b), with the global sea-level maximum reaching –10 to –20 m at 100 and 83 ka, respectively (Fig. 1e). These two warm intervals featured unstable ice-sheet configurations in Fennoscandia, Greenland, and North America (Chapman and Shackleton, 1999; Mokeddem and McManus, 2016; Batchelor et al., 2019). Ice-sheet instability and the associated meltwater input in the North Atlantic may have resulted in multi-centennial to millennial oscillations in Asian stalagmite  $\delta^{18}\text{O}$  values associated with Asian monsoon intensity variations (Cheng et al., 2016) (Fig. 1b). Fluctuations in Atlantic planktic foraminiferal  $\delta^{18}\text{O}$  ( $\delta^{18}\text{O}_{\text{pf}}$ ) values (Fig. 1c; de Abreu et al., 2003) and sea surface temperatures (SST) off the Iberian margin

(Fig. 1c; Martrat et al., 2004) during MIS 5c and 5a also suggest variations in the Atlantic meridional overturning circulation (AMOC), which can modulate the hydroclimate of the North Atlantic and Europe (Stouffer et al., 2006; Margari et al., 2010; Kageyama et al., 2013; Jackson et al., 2015; Stockhecke et al., 2016; Tzedakis et al., 2018). For example, abrupt  $\delta^{18}\text{O}$  shifts in Alpine stalagmite records (NALPS; Fig. 1d) which correspond to the  $\delta^{18}\text{O}$  shifts in Greenland ice cores (Fig. 1a; NorthGRIP-Members, 2004) could have been affected by ocean circulation changes (Boch et al., 2011). At the end of MIS 5b (~85 ka), the abrupt positive shift in NALPS  $\delta^{18}\text{O}$  has been linked to the end of GS22, accompanying warming in the North Atlantic (Boch et al., 2011).

The circum-Mediterranean region has a classical Mediterranean climate featuring hot/dry summers and mild/wet winters (Beck et al., 2018). Over the past two decades, droughts in southern Europe have threatened water supply, ecosystem, and agricultural instabilities over the past two decades (Hoerling et al., 2012; Naumann et al., 2021). Complex forcings from rising greenhouse gases, ice-sheet meltwater input, and changes in the strength of

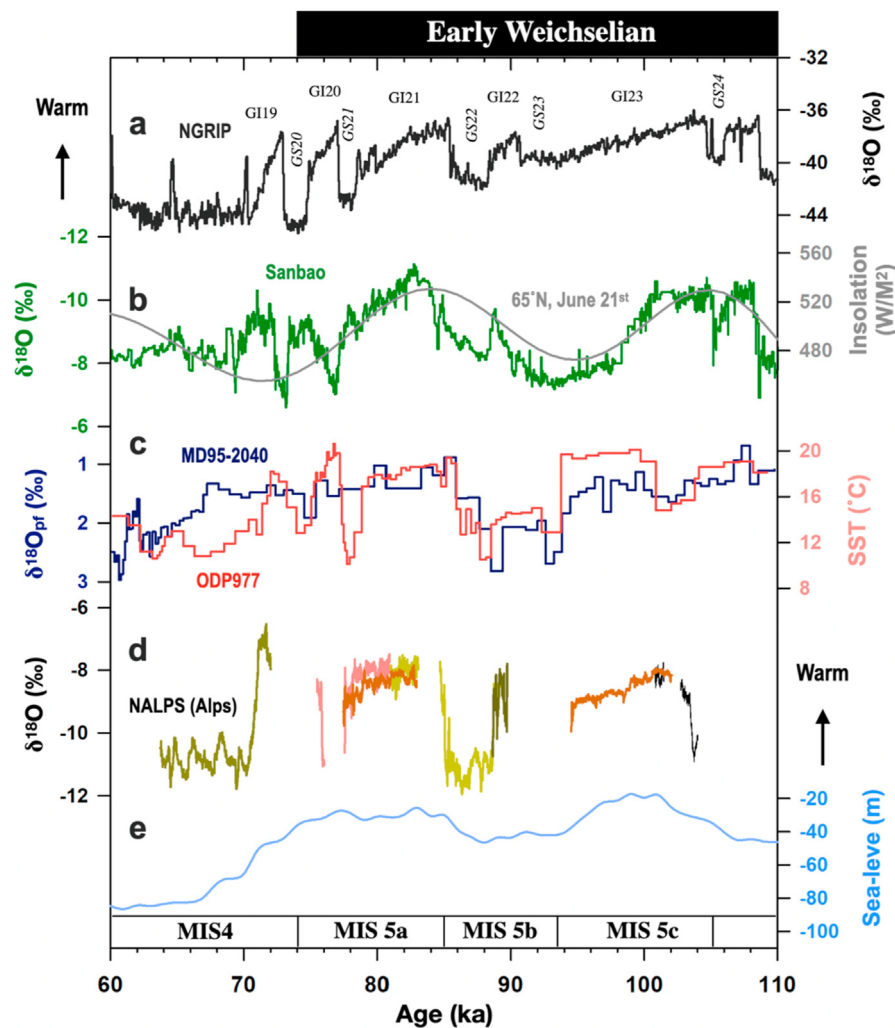


**Fig. 1.** Paleoclimate records during the early Weichselian. (a)  $\delta^{18}\text{O}$  values in NGRIP Greenland ice core (NorthGRIP-Members, 2004). High  $\delta^{18}\text{O}$  values imply warm climate in the N Atlantic. GI: Greenland interstadial. GS: Greenland stadial. (b) Grey: North hemisphere insolation at 65°N, June 21st (Laskar et al., 2011). Green: Stalagmite  $\delta^{18}\text{O}$  from Sanbao cave, China, as a proxy for Asian summer monsoon intensity (Cheng et al., 2016). Negative  $\delta^{18}\text{O}$  values represent a strong Asian summer monsoon. (c) Orange: sea surface temperature (SST) from marine core ODP977 at Iberia (Martrat et al., 2004). Dark blue: Planktonic foraminiferal  $\delta^{18}\text{O}$  ( $\delta^{18}\text{O}_{\text{pf}}$ ) from marine core MD95-2040 (de Abreu et al., 2003). (d) Stalagmite  $\delta^{18}\text{O}$  from the Alps (NALPS) (Boch et al., 2011). High  $\delta^{18}\text{O}$  values indicate warm conditions. (e) Global stacked sea level record (Spratt and Lisiecki, 2016). (For interpretation of the references to color in this figure legend, the reader is referred to the Web version of this article.)

AMOC hinder our ability to reliably predict Mediterranean hydroclimate over the next century. As NHSI values during MIS 5a are as high as those in the Holocene (Berger, 1978; Laskar et al., 2011), highly-resolved proxy records during MIS 5a offer important clues to better understand the future climate. Previous studies have highlighted centennial-to-millennial scale climatic variability in the North Atlantic during MIS 5 (e.g., Oppo et al., 1997; Mokeddem and McManus, 2016), especially in southern Europe (Denniston et al., 2018; Tzedakis et al., 2018; Budsky et al., 2019). Most cases, however, have focused on the Eemian warm period (MIS 5e; e.g., Tzedakis et al., 2003, 2018; Drysdale et al., 2005; Allen and Huntley, 2009; Milner et al., 2013;). Less attention has been given to subcentennial-to centennial-scale variability during MIS 5a due to the limitation of archive resolution and dating precision.

Here, we present a subdecadal-to multidecadal-resolved stalagmite-inferred precipitation record with robust chronology, from Monaco (northern Mediterranean) to understand hydroclimate variability associated with the westerly changes during 88.7–80.3 ka in the early Weichselian, especially focusing on MIS 5a. This is complemented by results from a transient experiment for the period 86–80 ka performed with the Earth system model (LOVECLIM), to assess the potential hydroclimatic variability drivers in southern Europe.

## 2. Material and methods

### 2.1. Cave and regional settings

Observatoire cave ([43°43' N, 7°24' E], 103 m above sea level) (Figs. 2 and 3) preserves evidence of the oldest human occupations in Monaco, southern Europe (Rossoni-Notter et al., 2016). The cave

is located along the northwestern Mediterranean coastline, in upper Jurassic bedrock - a limestone block from the “Arc de Nice” subalpine mountain chain (Gilli, 1999). This 600 m-long cave opens to the south and its entrance hall is 17 m in length, 6 m in width, and 7 m in height (Fig. 3a). After the entrance, the cave splits into two long and narrow 500 m passages, 1–2 m in width and height, with an innermost chamber, 5 m in width and 6 m in height at the terminus (Fig. 3a). A thin 0–5-cm clay soil lies above the 90 m cap rock of Jurassic limestone.

The average annual rainfall and temperature during AD 2003–2012 was  $631 \pm 400$  mm ( $1\sigma$ ) and  $21.1 \pm 2.6$  °C ( $2\sigma$ ; Monaco weather station, [43°43' N, 7°24' E], 131 m above sea level, 1 km from the cave), with monthly temperatures ranging from 9 to 37 °C. Modern climate in Monaco is a typical Mediterranean climate with hot/dry summers and mild/wet winters. Over 80% of the annual precipitation, brought by prevailing westerly winds, falls between September and February. The cave is situated in the transition zone between the subtropical high-pressure belt and the westerlies. During summer, a subtropical high-pressure system promotes dry sinking air and causes regional arid conditions. In the winter, precipitation is supplied from the westerlies and winter storms (García-Ruiz et al., 2011).

### 2.2. Samples and U–Th dating

Two candle-shaped stalagmites, OV12-1 and OV12-5, were collected from Observatoire cave ([43°43' N, 7°24' E], 103 m above sea level) (Fig. 3) in November 2012. OV12-1 is a 350-mm-long calcitic stalagmite (Fig. 3b) and OV12-5 a 180 mm-long aragonitic stalagmite (Fig. 3c). The collection chamber features high humidity (98–100%) and an annual temperature of 18.5 °C, within the

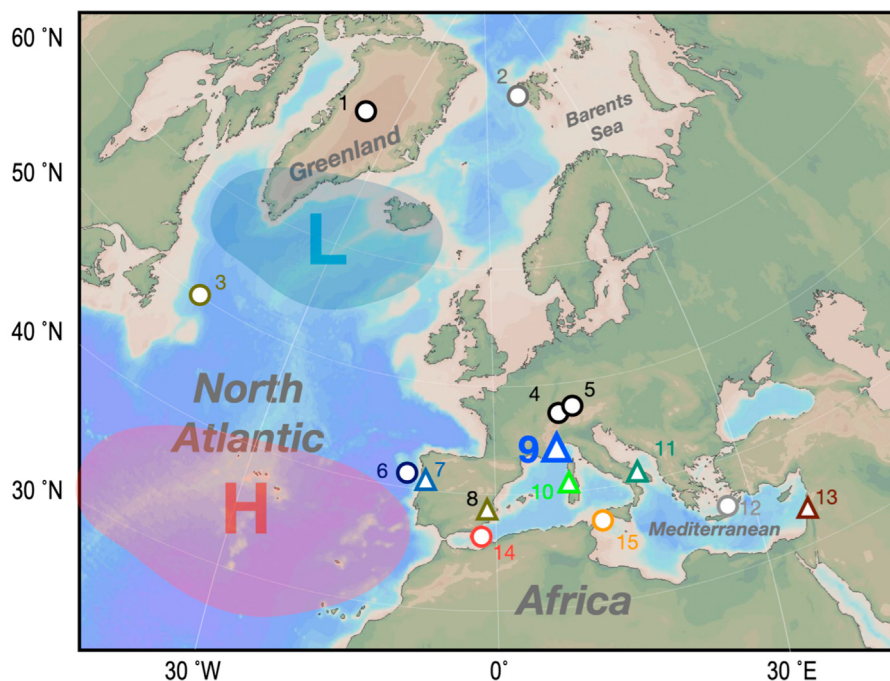


**Fig. 2.** Locations of Observatoire cave and other terrestrial and marine sites mentioned in this text. Triangles and circles denote cave records and other sites, respectively. 1. Greenland ice core NGRIP (NorthGRIP-Members, 2004; Wolff et al., 2010). 2. Marine sediment core MD99-2304 (Risebrobakken et al., 2005). 3. Marine cores U1302 and U1303 (Channell et al., 2012). 4 and 5. Beatus cave (Switzerland), Baschg cave (Austria), Klaus-Cramer- and Schneckenloch caves. All contribute to NALPS records (Boch et al., 2011). 6. Marine core MD95-2040 (de Abreu et al., 2003). 7. Buraca Gloriosa cave, Portugal (Denniston et al., 2018). 8. Cueva Victoria cave, Spain (Budsky et al., 2019). 9. Observatoire cave, Monaco (this study). 10. Crovassa Azzurra cave, Sardinia (Columbu et al., 2019). 11. Pozzo Cucù cave, southern Italy (Columbu et al., 2020). 12. Marine sediment core LC21 (Grant et al., 2012). 13. Soreq cave, Israel (Bar-Matthews et al., 2003). 14. Marine core ODP977 (Martrat et al., 2004). 15. Marine sediment core ODP963 (Sprovieri et al., 2006). Blue and red shades indicate the schematic positions of the Icelandic Low and the Azores High, respectively. Map was generated using Ocean Data View. (For interpretation of the references to color in this figure legend, the reader is referred to the Web version of this article.)

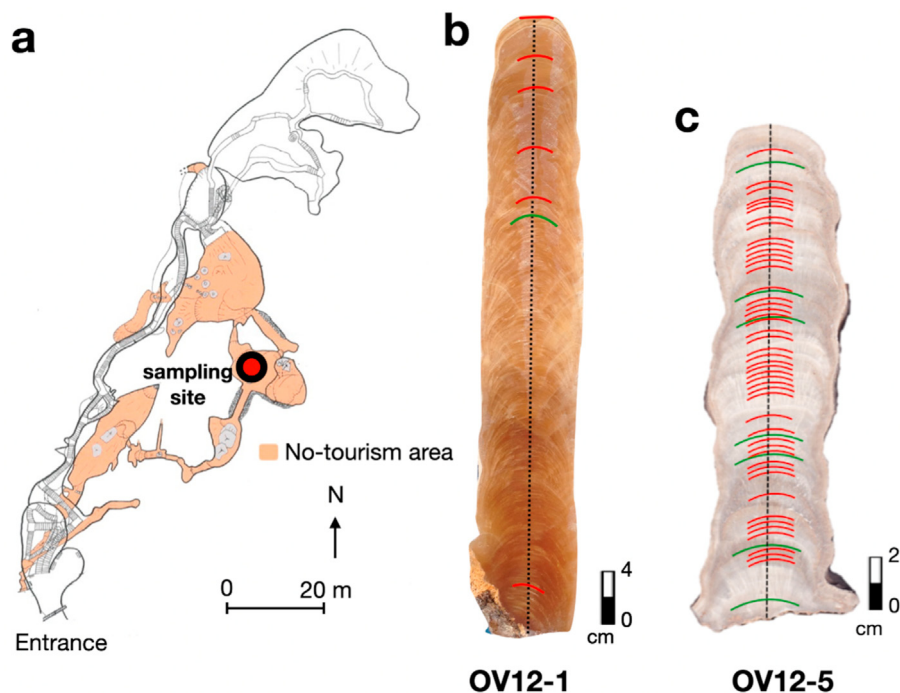


**Fig. 3.** Cave map and stalagmites. (a) Sketch map of Observatoire cave. Red circle indicates the location of stalagmites OV12-1 and OV12-5. Photographs of (b) OV12-1 and (c) OV12-5. In (b) and (c), Green lines represent layers for the Hendy test (Hendy, 1971). Subsamples for  $\delta^{13}\text{C}$  and  $\delta^{18}\text{O}$  analyses were drilled from the black dashed line along the central growth axis. Red layers are depths for U–Th dating. (For interpretation of the references to color in this figure legend, the reader is referred to the Web version of this article.)

modern range of  $21.1 \pm 2.6$  °C ( $2\sigma$ , AD 2003–2012). Both stalagmites feature clear growth bands with milky white and light tan layers, without visible porosity or detritus.

Five powdered subsamples, 50 mg each, were drilled from OV12-1 and forty-seven chipped subsamples, 75–230 mg each, were cut from OV12-5 for U–Th chemistry and instrumental analyses (Fig. 3b and c). Chemistry procedure was performed on class-100 benches in the class-10000 subsampling room at the High-Precision Mass Spectrometry and Environment Change Laboratory (HISPEC), Department of Geosciences, National Taiwan University (NTU) (Shen et al., 2003, 2008). U and Th isotopic compositions were measured on a multiple collector inductively coupled plasma mass spectrometer, Thermo-Fisher Neptune at the NTU. A dry sample introduction system, Cetec Aridus, was used (Shen et al., 2012). Half-lives of U–Th nuclides used are listed in Cheng et al. (2013).  $^{230}\text{Th}$  age was calculated using an assumed initial atomic  $^{230}\text{Th}/^{232}\text{Th}$  ratio of  $4 (\pm 2) \times 10^{-6}$ . Uncertainties in the isotopic data and  $^{230}\text{Th}$  dates are given at two-sigma ( $2\sigma$ ) uncertainty level or two standard deviations of the mean ( $2\sigma_m$ ). StalAge algorithm techniques (Scholz and Hoffmann, 2011) were used to build age model.

### 2.3. C/O stable isotope analysis

One layer on OV12-1 at 130 mm from the top and seven layers on OV12-5 at 14, 60, 70, 114, 120, 156, and 178 mm from the top were selected for the Hendy test (Hendy, 1971) (Fig. 3b and c), with five to seven coeval powdered subsamples on each layer. A total of 238 powdered subsamples on OV12-1 at 1-mm intervals and 710 powdered subsamples on OV12-5 at 0.1–1.0 mm intervals, 50–100  $\mu\text{g}$  each, drilled along the central growth axis on the polished surface (Fig. 3b and c) using a 0.2-mm dental drill, were analyzed. Instrumental measurements were conducted on a Micromass IsoPrime isotope ratio mass spectrometer at the Stable

Isotope Laboratory of the Department of Earth Sciences, National Taiwan Normal University, and on a Finnigan MAT 253 IRMS connected to an on-line, automated carbonate preparation system, Gasbench II, at the College of Geography Science, Fujian Normal University. Stable oxygen and carbon isotope values are reported as  $\delta^{18}\text{O}$  and  $\delta^{13}\text{C}$ , respectively, relative to the reference standard, Vienna Pee Dee Belemnite (VPDB), calibrated with the NBS-19 standard ( $\delta^{18}\text{O} = -2.20\text{‰}$ ). One-sigma external errors of  $\delta^{18}\text{O}$  and  $\delta^{13}\text{C}$  measurements were  $\pm 0.12\text{‰}$  and  $\pm 0.06\text{‰}$ , respectively.

### 2.4. Model simulation

A transient simulation of MIS 5 was performed with the earth system model of intermediate complexity LOVECLIM (Goosse et al., 2010). This simulation includes an ocean general circulation model ( $3 \times 3^\circ$  and 20 vertical levels), a dynamic thermodynamic sea-ice model, a quasi-geostrophic T21 atmospheric model, as well as a land surface scheme and a vegetation model (VECODE). This model is forced by transient changes in orbital parameters (Berger, 1978), greenhouse gases (Köhler et al., 2017), northern hemispheric ice-sheet, and associated albedo (Abe-Ouchi et al., 2007). The experiment starts at MIS 5e (Tzedakis et al., 2018) and was integrated forward in time until 80 ka, to investigate the impact of changes in boundary conditions on climate across MIS 5a.

## 3. Results

### 3.1. U–Th data and age model

Detailed U–Th isotopic and concentration data and dating results of Observatoire stalagmites OV12-1 and 12-5 are given in Table S1. Stalagmite OV12-1 has  $^{238}\text{U}$  content of  $0.4\text{--}0.7 \times 10^{-6}$  g/g and  $^{232}\text{Th}$  context of  $10\text{--}2200 \times 10^{-9}$  g/g. Stalagmite OV12-5 features high  $^{238}\text{U}$  contents of  $1.5\text{--}8.5 \times 10^{-6}$  g/g and low  $^{232}\text{Th}$

contents of  $0.01\text{--}2.1 \times 10^{-9}$  g/g. The uncertainties of corrected  $^{230}\text{Th}$  dates are from  $\pm 368$  to  $\pm 597$  years on OV12-1 and from  $\pm 19$  to  $\pm 180$  years on OV12-5. The dates are in stratigraphic order except for one outlier on OV12-5 at 136 mm ( $\sim 82.7$  ka) from the top. The uncertainties of StalAge model range from  $\pm 277$  to  $\pm 1723$  years (average  $\pm 486$  years) on OV12-1 (Fig. S1a) and  $\pm 10$  to  $\pm 176$  years (average  $\pm 48$  years) on OV12-5 (Fig. S1b). Stalagmite OV12-1 and OV12-5 deposited from  $88.8 \pm 0.4$  to  $82.0 \pm 1.7$  ka and  $83.6 \pm 0.2$  to  $80.3 \pm 0.1$  ka, respectively. The average growth rate is  $56 \mu\text{m/yr}$  for OV12-1 and  $54 \mu\text{m/yr}$  for OV12-5. No noticeable hiatus can be distinguished with the current age models (Fig. S1).

### 3.2. Stalagmite $\delta^{18}\text{O}$ and $\delta^{13}\text{C}$ time series

Results of stalagmite OV12-1 and 12–5  $\delta^{18}\text{O}$  and  $\delta^{13}\text{C}$  values are given in Table S2. The StalAge model reveals an average temporal resolution of 28 years for each stable isotope data point on OV12-1 and 5 years on OV12-5. The isotope series of OV12-1 and OV12-5 cover MIS 5b-5a and overlap from 83.7 to 81.7 ka. The  $\delta^{18}\text{O}$  values range from  $-6.5$  to  $-3.6\text{‰}$  on OV12-1 and from  $-4.6$  to  $-2.8\text{‰}$  on OV12-5 (Fig. 4a). OV12-1  $\delta^{18}\text{O}$  display millennial fluctuations with relatively high values of  $-3.8\text{‰}$  centered at  $87 \pm 0.4$  ka. OV12-5  $\delta^{18}\text{O}$  record shows a  $1.2\text{‰}$  increase from  $-4.6$  to  $-3.4\text{‰}$  between  $83.5 \pm 0.1$  and  $82.9 \pm 0.1$  ka, a  $0.7\text{‰}$  decrease from  $82.9 \pm 0.1$  to  $82.8 \pm 0.1$  ka, and then a  $0.9\text{‰}$  increase from  $82.8 \pm 0.1$  to  $82.5 \pm 0.1$  ka. Between  $82.5 \pm 0.1$  ka and  $80.5 \pm 0.1$  ka,  $\delta^{18}\text{O}$  data hovers between  $-4.1$  and  $-2.8\text{‰}$ , with  $0.8\text{--}1.2\text{‰}$  fluctuations on a multi-centennial timescale.

OV12-1  $\delta^{13}\text{C}$  data range from  $-10.1$  to  $-8.1\text{‰}$  and OV12-5  $\delta^{13}\text{C}$  from  $-7.6$  to  $-6.4\text{‰}$  (Fig. 4b). OV12-1  $\delta^{13}\text{C}$  record reveals relative positive values of average  $-8.8\text{‰}$  from  $88.8 \pm 0.4$  to  $85.6 \pm 0.3$  ka and relative negative values of average of  $-9.7\text{‰}$  from  $84.0 \pm 0.5$  to  $82.0 \pm 1.7$  ka. Both  $\delta^{13}\text{C}$  records are characterized by clear multi-centennial timescale variability.

We adopted the method described by Fohlmeister (2012) to combine the OV12-1 and OV12-5 stalagmite records. OV12-1 was tuned to the OV12-5  $\delta^{18}\text{O}$  record, at a 95% confidence level (Fig. 4a). The OV12-1  $\delta^{13}\text{C}$  record using the  $\delta^{18}\text{O}$ -tuned age is shown in Fig. 4b. The tuning method utilizes a Monte Carlo approach to optimize the correlation between the two series.

### 3.3. Climate simulations

Simulated AMOC strengths are presented in a six thousand year-long window at  $86\text{--}80$  ka in Fig. 5b. The modelled regional precipitation series on the  $[42\text{--}46^\circ\text{N}, 5\text{--}10^\circ\text{E}]$  sector is plotted in Fig. 5c and simulated Greenland temperature record in Fig. 5a. The two records (Fig. 5b and c) show that multi-centennial regional hydrological changes in Monaco are synchronous with those of AMOC strength in the North Atlantic. Atmosphere pressure field and wind field anomalies from two 200 year-long intervals with weak AMOC and with strong AMOC are illustrated in Fig. 5d and e.

## 4. Discussion

### 4.1. Tests for stalagmite isotopic equilibrium conditions

Factors affecting isotopic compositions in stalagmites depend on a variety of isotopic fractionation processes during rainfall condensation and water infiltration in karst systems (McDermott, 2004). Unexpected kinetic effects that are usually associated with degassing during carbonate precipitation could bias the isotope signals from the climatic imprint. The Hendy test (Hendy, 1971) and duplication test (Dorale and Liu, 2009) have been widely used for evaluating isotopic equilibrium. The results of the Hendy tests in

this study all show a 1-sigma variations of less than  $\pm 0.13\text{‰}$  for  $\delta^{18}\text{O}$  (Fig. S2a) and  $\pm 0.16\text{‰}$  for  $\delta^{13}\text{C}$  (Fig. S2b). On these layers, the absolute differences between the isotopic values,  $\delta^{18}\text{O}$  and  $\delta^{13}\text{C}$ , at  $\pm 2$  mm and center range from 0.01 to  $0.16\text{‰}$ , except for one layer at 178 mm (OV12-5), which has a difference of  $0.30\text{‰}$  for  $\delta^{18}\text{O}$  and  $0.39\text{‰}$  for  $\delta^{13}\text{C}$ . The standard deviations of all differences to center for all layers are  $\pm 0.09\text{‰}$  for  $\delta^{18}\text{O}$  and  $\pm 0.10\text{‰}$  for  $\delta^{13}\text{C}$ . Considering that the measurement external errors of  $\delta^{18}\text{O}$  and  $\delta^{13}\text{C}$  are  $\pm 0.12\text{‰}$  and  $\pm 0.06\text{‰}$ , respectively, the results suggest that kinetic fractionation is insignificant at an interval of  $\pm 2$  mm from the layer center.

Good agreement of concurrent variations between contemporaneous stalagmite OV12-1 and OV12-5  $\delta^{18}\text{O}$  records during  $83.7\text{--}81.7$  ka satisfy a sound duplication test (Dorale and Liu, 2009). The agreement indicates little kinetic effect on  $\delta^{18}\text{O}$  data. An observed  $\delta^{18}\text{O}$  offset of  $-1\text{‰}$  of calcitic OV12-1 is observed from aragonitic OV12-5. This offset can be attributed to different fractionation of  $0.6\text{--}1.4\text{‰}$  (Lachniet, 2009) between the calcite-water and aragonite-water system. The OV12-1  $\delta^{13}\text{C}$  values are  $2.5\text{‰}$  lower than those of OV12-5. This difference is compatible with reported calcite-aragonite offsets of between 1.1 and  $2.3\text{‰}$  (Romanek et al., 1992; Fohlmeister et al., 2018). The similarity of both  $\delta^{13}\text{C}$  records suggests that the  $\delta^{13}\text{C}$  time series captures environmental signals. In summary, the duplication between isotope records in OV12-1 and OV12-5 suggests an insignificant kinetic effect and implies that isotopic variations are mainly of environmental origin.

### 4.2. Climatic significance of $\delta^{18}\text{O}$ and $\delta^{13}\text{C}$

Mediterranean stalagmite  $\delta^{18}\text{O}$  could be controlled by various factors, such as dripwater  $\delta^{18}\text{O}$ , temperature, precipitation amount, and moisture source (e.g. Bar-Matthews et al., 1996; Mangini et al., 2005; Fairchild et al., 2006; Lachniet, 2009). Precipitation  $\delta^{18}\text{O}$  ( $\delta^{18}\text{O}_p$ ) mainly governs dripwater  $\delta^{18}\text{O}$  values that are eventually registered in the stalagmite. Based on modern observed precipitation data from Monaco (AD 1999–2016, GNIP-IAEA), the temperature effect on modern monthly  $\delta^{18}\text{O}_p$  data is  $0.30 \pm 0.10\text{‰}/^\circ\text{C}$  ( $2\sigma$ ,  $r = 0.42$ ,  $n = 177$ ,  $p < 0.01$ ) (Fig. S3a). This gradient is largely counterbalanced by the temperature-dependence fractionation of  $\sim -0.23\text{‰}/^\circ\text{C}$  (O'Neil et al., 1969). Considering estimated marine temperature changes of  $\sim 3^\circ\text{C}$  between 87.5 and 77.5 ka (Drysdale et al., 2020), the net temperature effect on speleothem  $\delta^{18}\text{O}$  is only  $\sim 0.1\text{‰}$  and negligible. Studies in the Mediterranean (Bar-Matthews and Ayalon, 2011; Domínguez-Villar et al., 2017; Baldini et al., 2019) also consider the regional temperature effect on Mediterranean stalagmite  $\delta^{18}\text{O}$  to be negligible.

The amount effect, which is a negative correlation between  $\delta^{18}\text{O}_p$  and rainfall amount due to vapor-water  $\delta^{18}\text{O}$  fractionation in air masses, is one of the key factors that control Mediterranean stalagmite  $\delta^{18}\text{O}$  (Ruan et al., 2016; Columbu et al., 2019, 2020; Regattieri et al., 2019; Thatcher et al., 2020a, 2020b). Monthly modern precipitation data (1999–2016 AD, GNIP-IAEA) indicate average values of  $-2.4 \pm 0.8\text{‰}$  per 100 mm/month precipitation ( $2\sigma$ ,  $r = 0.40$ ,  $n = 186$ ,  $p < 0.01$ ) (Fig. S3b), consistent with a simulated amount effect of  $-2.0 \pm 0.6\text{‰}$  per 100 mm/month (Bard et al., 2002) and regional mean values of  $-1.6 \pm 0.2\text{‰}$  per 100 mm/month in the western Mediterranean (Bard et al., 2002).

Precipitation originating from the Mediterranean region displays more positive  $\delta^{18}\text{O}$  values of  $-4.62\text{‰}$  (weighted mean) than from the Atlantic ( $-8.48\text{‰}$ ) (Celle-jeanton et al., 2001). Proportional changes of the moisture sourced from the two regions could alter  $\delta^{18}\text{O}_p$ . As Observatoire cave is located  $<100$  m from the coast, it receives Mediterranean-sourced moisture, and the “source effect” could be important on Observatoire stalagmite isotope records.

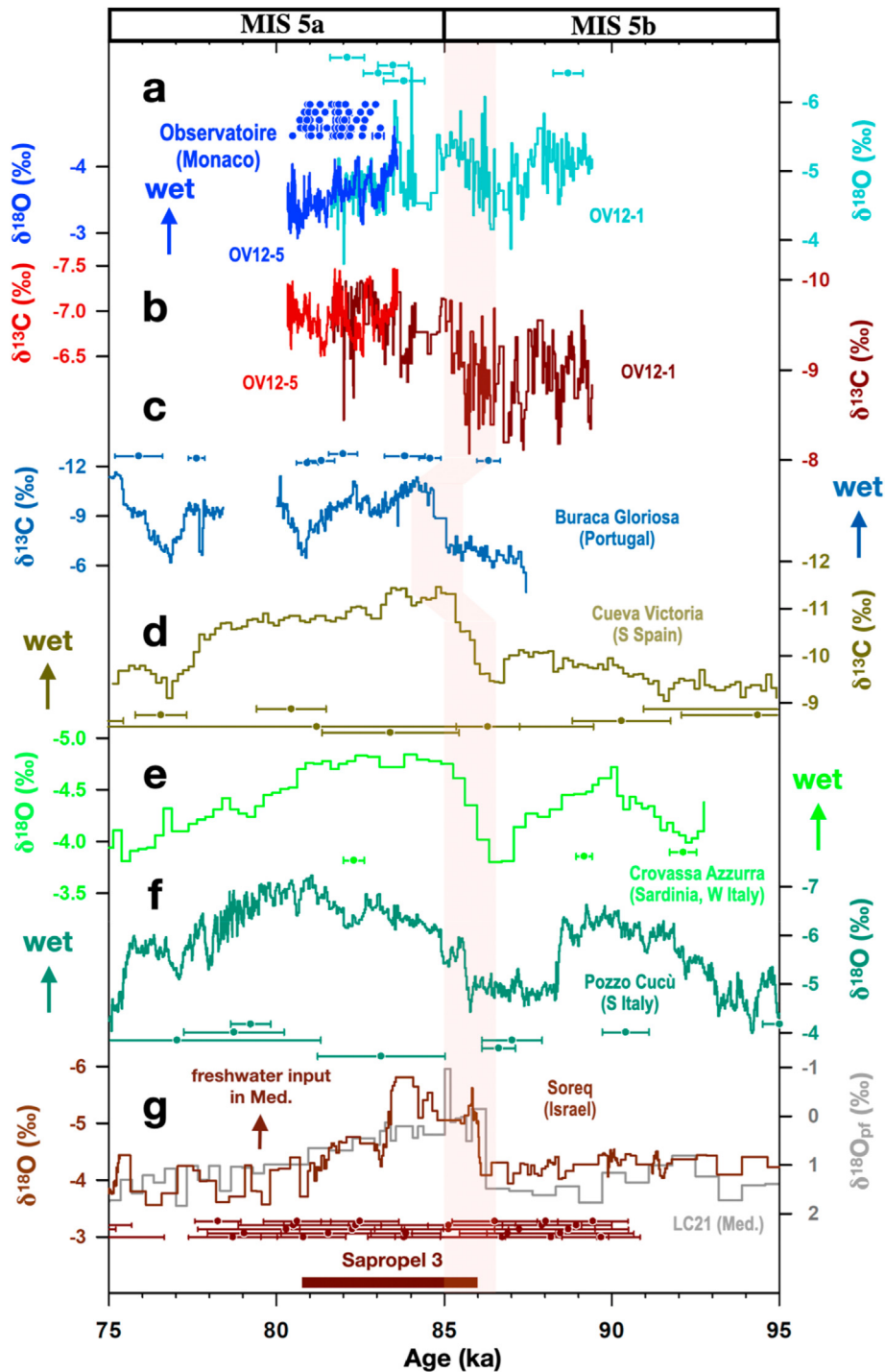


**Fig. 4.** Circum-Mediterranean paleoclimate records at 95–75 ka. (a) Tuned OV12-1 (tiffany) and OV12-5 (blue)  $\delta^{18}\text{O}$ . (b) Tuned OV12-1 (brown) and OV12-5 (red)  $\delta^{13}\text{C}$ . (c) Stalagmite  $\delta^{13}\text{C}$  from Buraca Gloriosa, Portugal (Denniston et al., 2018). (d) Stalagmite  $\delta^{13}\text{C}$  from Cueva Victoria, southern Spain (Budsky et al., 2019). (e) Stalagmite  $\delta^{18}\text{O}$  from Crovassa Azzurra, Sardinia (Columbu et al., 2019). (f) Stalagmite  $\delta^{18}\text{O}$  from Pozzo Cucù (Columbu et al., 2020). (g) Stalagmite  $\delta^{18}\text{O}$  from Soreq cave (brown; Bar-Matthews et al., 2003) and planktonic foraminiferal  $\delta^{18}\text{O}$  ( $\delta^{18}\text{O}_{\text{pf}}$ ) from marine LC21, Mediterranean Sea (Grant et al., 2012).  $^{230}\text{Th}$  ages and errors are color-coded by records. The vertical pink bar denotes the transition from MIS 5b to 5a. (For interpretation of the references to color in this figure legend, the reader is referred to the Web version of this article.)

While it is difficult to track moisture sources during MIS 5b–5a, modern Monaco precipitation is sourced primarily from the Atlantic, with minor Mediterranean or mixed sources (Columbu et al., 2019, 2020). Significant Mediterranean-sourced moisture can, however, be observed along with large ice-sheets (Merz et al., 2015; Drysdale et al., 2009). For example, the presence of the Laurentide ice-sheet could disturb Rossby wave configuration and

push the region where the eddies form equatorially (Merz et al., 2015; Ludwig et al., 2016), shifting westerly tracks towards the south and increasing Mediterranean-sourced moisture at Monaco (Luetscher et al., 2015). Strong AMOC, usually observed in warm periods, can lead to high moisture transport from the Atlantic into the Mediterranean (Sánchez Goñi et al., 1999), seen as relatively negative Mediterranean stalagmite  $\delta^{18}\text{O}$  (Drysdale et al., 2009;

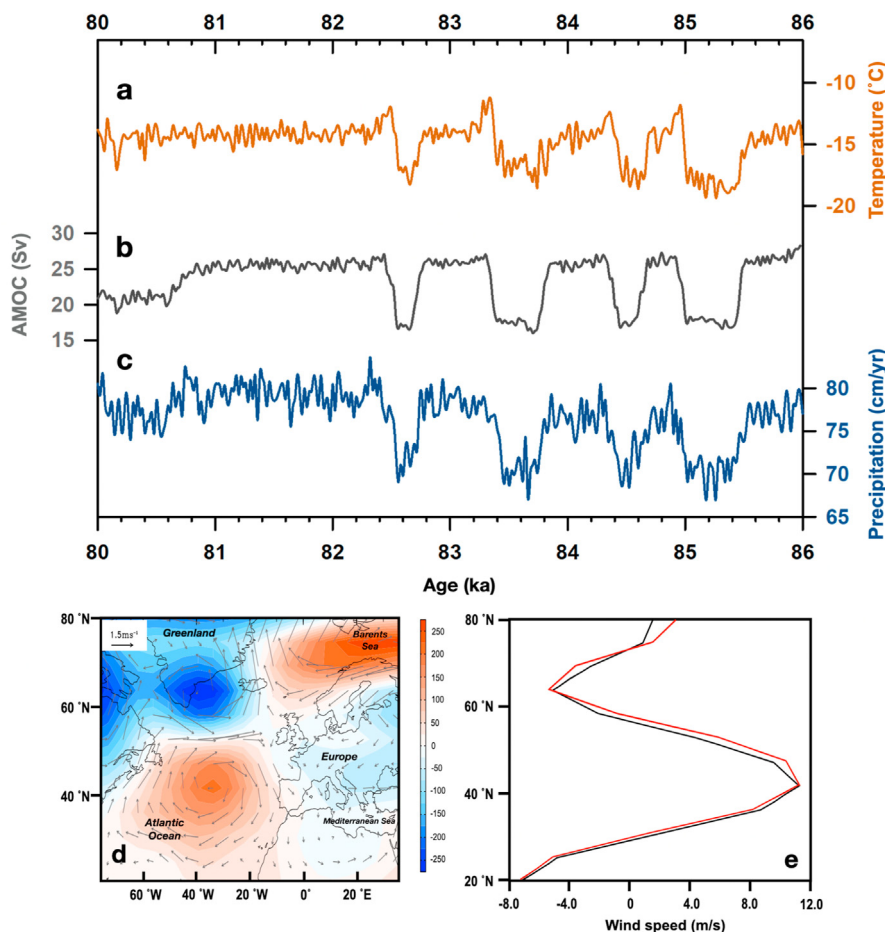


**Fig. 5.** Results of a transient experiment with LOVECLIM. (a) Simulated Greenland temperature variations. (b) Simulated AMOC (unit: Sv). (c) Simulated annual precipitation at [42–46°N, 5–10°E]. (d) 800 mb geopotential height (hPa, shades) and 800 mb wind (m/s, vectors) anomalies between winters (December–February) with weak AMOC and strong AMOC. (e) Zonal winter (December–February) wind speed at 800 mb averaged over the Atlantic basin [60°W–0] for periods with strong AMOC (black) and weak AMOC (red). (For interpretation of the references to color in this figure legend, the reader is referred to the Web version of this article.)

Dumitru et al., 2018). Intense vapor advection and high efficiency of Atlantic moisture transport can accompany strong westerly winds and high rainfall in Monaco, modulating  $\delta^{18}\text{O}_p$  in a negative way. Observatoire stalagmite  $\delta^{18}\text{O}$  can, therefore, be considered as a qualitative indicator of the strength of the westerlies at this region, with strong westerlies associated with intense precipitation and a high proportion of Atlantic-sourced moisture corresponding to low  $\delta^{18}\text{O}$ , and *vice versa*.

The source of carbon for stalagmites is soil  $\text{CO}_2$ , mainly governed by plant roots' respiration and organic matter decomposition. The roots form carbonic acid in contact with water, which dissolves cave host-rock (e.g., Columbu et al., 2018). Pedogenic carbonate  $\delta^{13}\text{C}$  values are related to surrounding vegetation (McDermott, 2004), such as C3 and C4 plants. The respective aragonitic OV12-1 and calcitic OV12-5  $\delta^{13}\text{C}$  values of  $-8.0$  to  $-10.4\text{‰}$  and  $-7.6$  to  $-6.5\text{‰}$  are within the predicted stalagmite  $\delta^{13}\text{C}$  range of  $-14$  to  $-6\text{‰}$  dominated by C3 type vegetation (McDermott, 2004), similar to the plants in Monaco today (Mediterranean bush). C3 plants dominated the land surface in the Mediterranean region during both glacial and interglacial periods (Columbu et al., 2020), and stalagmite  $\delta^{13}\text{C}$  during MIS 5b-5a was not dominated by vegetation shifts between C4 and C3 plants. OV12-5  $\delta^{13}\text{C}$  variations are mainly governed by soil microbial activity and/or vegetation density (Columbu et al., 2019, 2020), both affected by regional

alternation of wet/warm or dry/cold conditions in the Mediterranean. High soil microbial activity and dense vegetation can lead to negative stalagmite  $\delta^{13}\text{C}$  values.

Prior carbonate precipitation (PCP), a process of progressive  $\text{CO}_2$  degassing and carbonate formation in the percolation pathway, can also influence stalagmite  $\delta^{13}\text{C}$  (Fairchild et al., 2000). In wet (dry) conditions with high (low) precipitation, diminished (enhanced)  $\text{CO}_2$  degassing and short (long) water residence time during the pathway disfavor (favor) the formation of PCP, and then lower (elevate)  $\delta^{13}\text{C}$  in dripwater. Accordingly, multi-centennial  $\delta^{13}\text{C}$  variability in Observatoire stalagmite could mainly reflect precipitation changes and related bioproductivity. Low (high) stalagmite  $\delta^{13}\text{C}$  values reflect high (low) precipitation or bioproductivity.

Increasing rainfall can lower  $\delta^{18}\text{O}$  by the amount effect and  $\delta^{13}\text{C}$  by increasing soil moisture content and soil respiration rates or by reducing PCP, resulting in a positive correlation of  $\delta^{13}\text{C}$  and  $\delta^{18}\text{O}$ . OV12-5  $\delta^{13}\text{C}$  data express a degree of correlation with  $\delta^{18}\text{O}$  values ( $r = 0.48$ ,  $n = 710$ ,  $p < 0.05$ ), supporting our argument that stalagmite  $\delta^{18}\text{O}$  and  $\delta^{13}\text{C}$  reflect precipitation changes. General similarity of multi-centennial variations between records of carbon and oxygen isotopes on OV12-5 (Fig. S4a and b) and uranium concentration (Fig. S4c) could further support this argument. Uranium is easily leached out of bedrock and the high content in the stalagmite suggests enhanced water leaching associated with increased

precipitation. Initial  $\delta^{234}\text{U}$  ( $\delta^{234}\text{U}_{\text{initial}}$ ) (Fig. S4d) and growth rate (Fig. S4e) can sometimes be used to infer hydroclimate changes (e.g., Columbu et al., 2020). In Observatoire cave, however,  $\delta^{234}\text{U}_{\text{initial}}$  and growth rate are distinctively different from C/O isotopic time series (Fig. S4a, b, d and e), indicating additional complicated effects from changing redox conditions, percolation pathway on both, and possibly growth rate on  $\delta^{234}\text{U}$  (Zhou et al., 2005, Day and Henderson, 2013).

#### 4.3. Circum-Mediterranean climate patterns during MIS 5b–5a

Over the entire MIS 5 period, MIS 5b was notable as a cold period with minimum temperatures anchored around  $87.8 \pm 0.4$  ka (NorthGRIP-Members, 2004; Lisiecki and Raymo, 2005). MIS 5b ended at  $84.7 \pm 0.4$  ka, when NH summer insolation reached a maximum (Fig. 1b; NorthGRIP-Members, 2004; Laskar et al., 2011). At  $84.7 \pm 0.4$  ka, Greenland ice core  $\delta^{18}\text{O}$  feature a positive excursion (Fig. 1a), suggesting warming in the North Atlantic, concurrent with Iberian warming (Fig. 1c). In line with positive  $\delta^{18}\text{O}$  shifts in the NALPS stalagmite series at  $85.0 \pm 0.4$  ka (Fig. 1d), these geological proxy records confirm large-scale warming over the Atlantic-European sector during the transition from MIS 5b to 5a. During this transition, 87–85 ka, Observatoire stalagmite  $\delta^{18}\text{O}$  decreased (Fig. 4a), along with  $\delta^{13}\text{C}$  (Fig. 4b), suggesting increased precipitation at Monaco, similar to Portugal (Fig. 4c; Denniston et al., 2018), Spain (Fig. 4d; Budsky et al., 2019), Sardinia (Fig. 4e; Columbu et al., 2019) and southern Italy (Fig. 4f; Columbu et al., 2020), all with negative shifts in stalagmite  $\delta^{18}\text{O}$  and  $\delta^{13}\text{C}$ . The consistency suggests that westerly winds were enhanced in the Mediterranean at the onset of MIS 5a (Denniston et al., 2018; Budsky et al., 2019; Columbu et al., 2019, 2020). The increasing water budget in the Mediterranean realm and the concurrent strengthening of the African monsoon, and sea-level rise, may have been responsible for Sapropel event 3 (S3, 86–81 ka; Rohling et al., 2015). Increased  $^{18}\text{O}$ -depleted freshwater input into the Mediterranean region is manifest as a negative  $\delta^{18}\text{O}$  shift in Israel speleothems (Fig. 4g) and marine planktonic foraminifera from core LC21 (Fig. 4g; Grant et al., 2012; Rohling et al., 2015).

From the onset of MIS 5a, Portugal (Fig. 4c; Denniston et al., 2018) and Spanish (Fig. 4d; Budsky et al., 2019) stalagmite records both show relatively stable  $\delta^{13}\text{C}$  values until the end of S3 at 81 ka. Sardinia stalagmite  $\delta^{18}\text{O}$  (Fig. 4e; Columbu et al., 2019) display a persistent value of  $\sim -4.7\%$ , while southern Italy stalagmite  $\delta^{18}\text{O}$  (Fig. 4f; Columbu et al., 2020) show a depletion of  $\sim 1\%$ . Taken together, these records suggest that strong westerly winds may have prevailed during the whole of S3. These climate patterns are consistent with the relatively low  $\delta^{13}\text{C}$  values in OV12-5, as compared with those during MIS 5b (Fig. 4b).

The millennial increasing trend of  $\sim 1\%$  in the OV12-5  $\delta^{18}\text{O}$  record from 83.5 to 80.5 ka could be attributable to increasing Mediterranean seawater-sourced  $\delta^{18}\text{O}$ . This agreement is supported by a  $\sim 0.8\%$  enrichment in  $\delta^{18}\text{O}_{\text{pf}}$  of a Mediterranean sediment core, LC21, in Fig. 6g (Bar-Matthews et al., 2003; Grant et al., 2012), as the concurrent decrease of NHSI led to a weakened African monsoon that reduced the proportion of freshwater with depleted- $^{18}\text{O}$  in the Mediterranean Sea at the end of S3 (Rohling et al., 2015). Another possibility is an increase in Mediterranean-sourced moisture at the Monaco cave when the NHSI shifted the intertropical convergent zone southward, promoting more southerly water advections in southern Europe (Vanghi et al., 2018; Columbu et al., 2019).

#### 4.4. Multi-centennial dry events of early MIS 5a

Both OV12-5  $\delta^{18}\text{O}$  and  $\delta^{13}\text{C}$  series are characterized by four

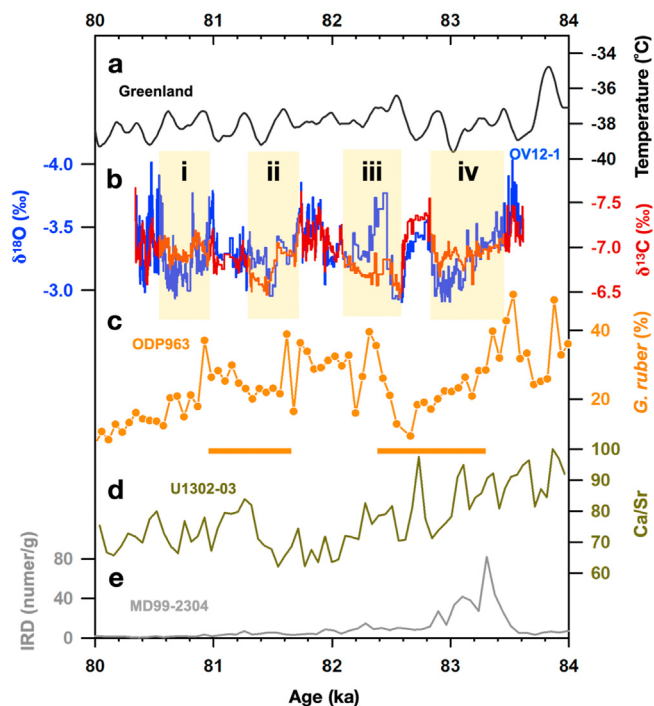


**Fig. 6.** North Atlantic proxy records during 84–80 ka. (a) Greenland NGRIP temperature reconstruction on the ss09sea06bm timescale (Kindler et al., 2014). (b) Stalagmite OV12-5  $\delta^{18}\text{O}$  (blue; detrended, this study) and  $\delta^{13}\text{C}$  (red). Light yellow bars denote dry events, i–iv, identified by stalagmite OV12-5 records. (c) Abundance percentage of *G. ruber* (orange) in marine core ODP963, Mediterranean Sea (Sprovieri et al., 2006). Orange bars indicate the periods with cooling in the North Atlantic, defined by Sprovieri et al. (2006). (d) Ca/Sr ratio in two marine cores of U1302 and U1303, North Atlantic, as proxy of ice-sheet melting histories (Channell et al., 2012). (e) Ice rafted debris (IRD) in marine core MD99-2304, Nordic sea (Risebrobakken et al., 2005). (For interpretation of the references to color in this figure legend, the reader is referred to the Web version of this article.)

concurrent multi-centennial high-value intervals, centered at  $83.1 \pm 0.1$ ,  $82.4 \pm 0.1$ ,  $81.6 \pm 0.1$ , and  $80.7 \pm 0.1$  ka (Fig. 6b, events i to iv). These events show multi-centennial dry conditions at MIS 5a in Monaco, probably caused by shifting of the westerlies. Similar drought 8.2-k and 4.2-k events in the Holocene (e.g., Ait-Brahim et al., 2019; Thatcher et al., 2020a, 2020b) were proposed to be caused by migrations of the westerlies under the changing phase of centennial North Atlantic Oscillation (NAO)-like states (Hurrell, 1995). A positive NAO state can enhance both the Icelandic Low and Azores High, and divert the westerlies towards northern Europe, resulting in dry climate in the Mediterranean (e.g., Ait-Brahim et al., 2019). Modern instrumental rainfall data around Monaco reveal a strong dipole correlation with zonal winds centered at  $\sim 42$  and  $\sim 62^\circ\text{N}$  (Fig. S5), suggesting that a latitudinal westerly migration could be an important factor in determining precipitation patterns in Monaco. Hence, we argue that the multi-centennial dry conditions recorded in OV12-5 isotopic records could be attributed to the drift of the westerlies.

Over centennial scales, studies have indicated that the westerlies could shift latitudinally under different Atlantic Multidecadal Oscillation states (e.g., Morley et al., 2014) or NAO (e.g., Deininger et al., 2017; Ait-Brahim et al., 2019). Meltwater input in the North Atlantic and Atlantic oceanic circulation changes could also alter westerly trajectories that penetrate into Europe (e.g., Wassenburg et al., 2016). During MIS 5a, some ice-sheet remnants still covered North America, Greenland, and northern Europe (Batchelor et al., 2019). The meltwater input from ice-sheets in the North



Atlantic and associated AMOC variations (e.g., Ait-Brahim et al., 2019) could contribute to the Monaco stalagmite-inferred dry events during the early MIS 5a (Fig. 5a).

#### 4.5. Connecting the multi-centennial dry events to Atlantic ocean circulation

The LOVECLIM simulation in Fig. 5a–c features multi-centennial scale AMOC reductions centered at 85.2, 84.5, 83.5, and 82.6 ka (Fig. 5b) associated with relatively cold conditions in Greenland (Fig. 5a) and dry conditions in southern Europe ([42–46°N, 5–10°E], Fig. 5c). The duration and frequency of multicontinental dry conditions observed in our simulation (Fig. 5c) are similar to those inferred from Observatoire stalagmite  $\delta^{18}\text{O}$  and  $\delta^{13}\text{C}$  records (Fig. 6b). One simulated cold period in the North Atlantic and dry phase in southern Europe centered at 83.5 ka generally matches the one recorded in marine sediment cores and stalagmite records (Fig. 6b–d).

Our model reveals an AMOC slowdown can trigger a deepened Icelandic Low and enhanced the Azores High in winter (December–February; Fig. 5d), as seen in Tzedakis et al. (2018). Simulated winter (December–February) zonal winds at 800 mb over the Atlantic basin [60°W–0] (Fig. 5d) reveal that the westerlies migrated slightly poleward when AMOC was weak. An enhanced Azores High connecting high pressures at Barents Sea is also observed (Fig. 5d). This atmospheric configuration could weaken the westerlies with moisture blowing into the northern Mediterranean region and most of mainland Europe (Ionita et al., 2016), as evidenced by negative (westward) wind anomalies at 45–55°N over Europe shown in our simulation (Fig. 5d).

Two cold periods inferred from low *Globigerinoides ruber* abundances of the marine sedimentary core ODP 963 in the central Mediterranean at 83.5–82.5 ka and 81.6–81.1 ka, defined by Sprovieri et al. (2006) (orange intervals in Fig. 6c), match dry events ii and iv observed in Observatoire records (Fig. 6b). These two events are also synchronous with cold periods identified in the western Atlantic (Heusser and Oppo, 2003) and recorded in Greenland ice cores (Fig. 6a) (Kindler et al., 2014). The cooling events in the high-latitude North Atlantic and arid events in southern Europe could be attributable to periods with weakened AMOC. A weakened AMOC could also explain concurrent relatively high Ca/Sr ratios in marine cores of U1302 and U1303, which are associated with enhanced meltwater input and detrital carbonate in the Atlantic (Fig. 6d; Channell et al., 2012). Similar to the Holocene and the last glacial cycle, these AMOC slowdowns are not necessarily associated with ice-rafted detrital (IRD) events (Channell et al., 2012; Ait-Brahim et al., 2019). Indeed, only one IRD event was registered in marine core MD99-2304 from the Nordic Sea (Fig. 6e; Risebrobakken et al., 2005) with high values at 83.6–82.8 ka and no other IRD events were discovered so far in the rest of MIS 5a.

Stalagmite-inferred droughts i and iii (Fig. 6b) was not captured by marine records, probably attributable to relatively low temporal resolution and chronology uncertainty. They could be still induced by centennial-scale intrinsic AMOC variability. Previous studies suggest that the triggering of internally generated AMOC could be initiated by stochastic atmospheric forcing (Drijfhout et al., 2013; Kleppin et al., 2015), with enhanced atmospheric blocking over the eastern subpolar gyre inducing a southward progression of the sea-ice margin. Another possible process is linked to stochastic changes in sea ice (Friedrich et al., 2010). Sea ice shifts that cover a large portion of the sinking region could cause a reduction in the strength of overturning. For example, Yin et al. (2021) highlighted a major centennial-scale AMOC periodicity induced by the interaction between sea ice and ocean circulation. AMOC can be weakened

when sea ice in Nordic Sea increases and impedes overturning, as the Nordic Sea is one of the major sinking areas for AMOC. Once AMOC slows, ocean heat accumulates in the subsurface seawater and the heat further elevates sea temperature. As surface waters warm, sea ice in the Nordic Sea could melt again, increasing overturning.

#### 4.6. Other possible forcings for centennial Monaco hydroclimate changes

Model simulations show that AMOC slowdowns lead to distinct air temperature drops over Greenland (Fig. 5a and b). However, low Greenland temperature is observed at events ii and iv, but only slightly observed at drought event i and obscure during event iii (Fig. 6a and b). We argue that centennial NAO-state variations could also induce low precipitation in southern Europe in addition to the occurrence of AMOC slowdown. Ait Brahim et al. (2019) proposed that a positive-NAO-like condition lead to a northward shift of the westerlies and centennial-scale dry conditions in western and northern Mediterranean regions in the Holocene. The NAO-correlated 100s-yr dry events are also observed since the middle Holocene in stalagmite  $\delta^{18}\text{O}$  records from Bäsura cave in northern Italy (Hu et al., 2022), where is located in the same climate territory

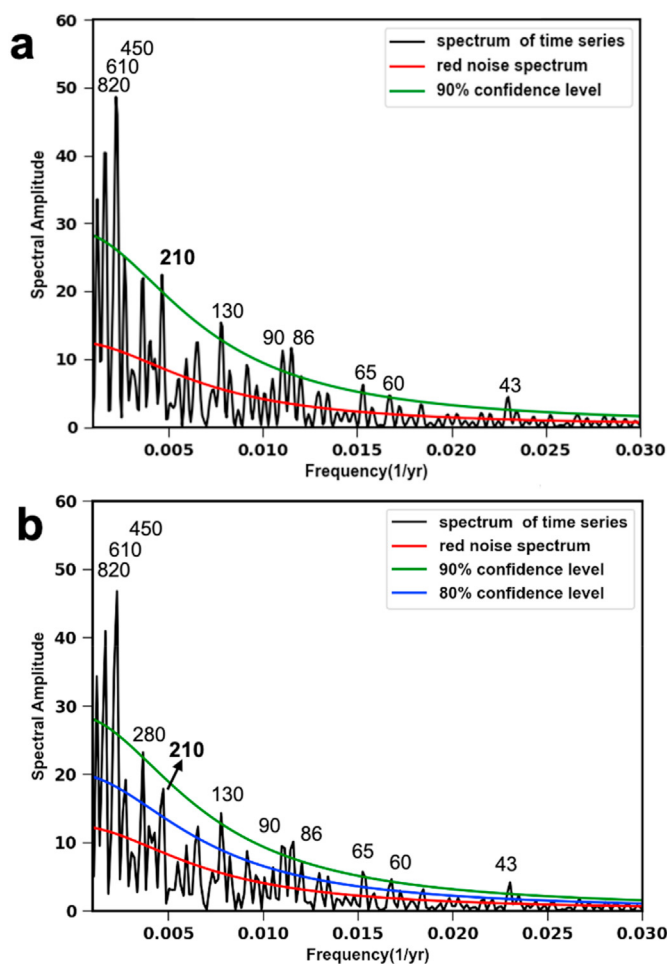


Fig. 7. Results of spectral analyses for Observatoire OV12-5 isotope time series. (a)  $\delta^{18}\text{O}$  and (b)  $\delta^{13}\text{C}$  spectral amplitude against red noise (Schulz and Mudelsee, 2002). Numbers indicate periodicities in years for the peak. (For interpretation of the references to color in this figure legend, the reader is referred to the Web version of this article.)

of Observatoire cave in Monaco. The evidence supports that change in NAO phase could be one of forcings to cause multi-centennial arid intervals at MIS 5a expressed in Fig. 6b.

Spectral analyses of Observatoire  $\delta^{18}\text{O}$  and  $\delta^{13}\text{C}$  records (Fig. 7) show several significant multi-decadal to multi-centennial periodicities. A 210-year periodicity is revealed in both  $\delta^{18}\text{O}$  (Fig. 7a) and  $\delta^{13}\text{C}$  (Fig. 7b) above the 90% and 80% confidence levels, respectively. This bicentennial cycle is close to the De Vries-Suess 210-year solar cycle (Suess, 1980) and was not observed in existing MIS 5a proxy records. Previous studies have revealed the similar impact of solar activity on the regional Holocene hydroclimate in the western Mediterranean (e.g., Frisia et al., 2003; Scholz et al., 2012; Smith et al., 2016; Ait-Brahim et al., 2018, 2019). For example, the 210-year periodicity is observed in the Holocene stalagmite  $\delta^{18}\text{O}$  record from northern Morocco (Ait-Brahim et al., 2019). During solar minima, an enhanced blocking frequency at Greenland could shift the westerly trajectory towards the Mediterranean region, resulting in more precipitation in the western Mediterranean (Ait-Brahim et al., 2019). The downward-propagation of the solar signal from the stratosphere to the surface induces a southward shift of the northern subtropical jet and a decrease in temperature in northern high latitudes (Bond et al., 2001; Kodera, 2002; Thiéblemont et al., 2015; Yukimoto et al., 2017). Our stalagmite records suggest that centennial-scale hydroclimate oscillations at MIS 5a in Monaco could also be influenced by solar activity (Ait-Brahim et al., 2019), as the case in the Holocene.

## 5. Conclusions

We present stalagmite  $\delta^{18}\text{O}$  and  $\delta^{13}\text{C}$ -inferred precipitation records from  $88.7 \pm 0.4$  to  $80.3 \pm 0.1$  ka covering parts of MIS 5b to 5a from Observatoire cave, Monaco, southern Europe. The inferred precipitation record features four multi-centennial arid events during MIS 5a, suggesting that the westerlies moved away from Monaco. New transient simulation suggests that AMOC slowdowns can divert the westerlies from the Mediterranean region, which would result in stalagmite-inferred dry conditions in Monaco. A positive NAO-like scenario is also one possible forcing. A bicentennial periodicity revealed in Observatoire isotope records highlight the potential of additional solar forcing on Mediterranean hydroclimate during MIS 5a. Our findings provide a clue for future climate prediction as the AMOC was observed to slow down over the past decade (Smeed et al., 2018).

## Author contributions

C.-C.S. directed this research. C.-C.S., Y.-C.C. and H.-M.H. conceived the project. C.-C.S., V.M., P.V., P.S., E.R.-N., A.M. and C.-C.W. conducted field surveys and collected stalagmites. Y.-C.C. and H.-M.H. conducted subsample preparation. Y.-C.C. and H.-M.H. performed U–Th dating. H.-S.M. and X.J. conducted carbon and oxygen stable isotope analyses. L.M. conducted model simulations. A.M. conducted statistical analyses. Y.-C.C., C.-C.S., H.-M.H., L.M., and H.S. prepared the draft and interpretations, and all authors contributed to manuscript completion.

## Declaration of competing interest

The authors declare that they have no known competing financial interests or personal relationships that could have appeared to influence the work reported in this paper.

## Acknowledgments

We would like to deeply thank G.S. Burr of the Research Center for Future Earth, National Taiwan University, for his constructive suggestions. We are thankful for the financial support provided by grants from the Science Vanguard Research Program of the Ministry of Science and Technology, Taiwan, ROC (110-2123-M-002-009), the Higher Education Sprout Project of the Ministry of Education, Taiwan, ROC (110L901001 and 110L8907), and the National Taiwan University (109L8926). We are also grateful the Government of Monaco and the Museum of Prehistoric Anthropology of Monaco for the sample collections. L.M. acknowledges support from the Australian Research Council, grant FT180100606.

## Appendix A. Supplementary data

Supplementary data to this article can be found online at <https://doi.org/10.1016/j.quascirev.2022.107581>.

## References

- Abe-Ouchi, A., Segawa, T., Saito, F., 2007. Climatic conditions for modelling the Northern Hemisphere ice sheets throughout the ice age cycle. *Clim. Past* 3, 423–438.
- Ait Brahimi, Y., Wassenburg, J.A., Sha, L., Cruz, F.W., Deininger, M., Sifeddine, A., Bouchaou, L., Spötl, C., Edwards, R.L., Cheng, H., 2019. North Atlantic ice-rafting, ocean and atmospheric circulation during the Holocene: insights from western Mediterranean speleothems. *Geophys. Res. Lett.* 46, 7614–7623.
- Ait Brahimi, Y., Wassenburg, J.A., Cruz, F.W., Sifeddine, A., Scholz, D., Bouchaou, L., Dassié, E.P., Jochum, K.P., Edwards, R.L., Cheng, H., 2018. Multi-decadal to centennial hydro-climate variability and linkage to solar forcing in the Western Mediterranean during the last 1000 years. *Sci. Rep.* 8, 1–8.
- Allen, J.R., Huntley, B., 2009. Last Interglacial palaeovegetation, palaeoenvironments and chronology: a new record from Lago Grande di Monticchio, southern Italy. *Quat. Sci. Rev.* 28, 1521–1538.
- Baldini, L.M., Baldini, J.U., McDermott, F., Arias, P., Cueto, M., Fairchild, I.J., Hoffmann, D.L., Matthey, D.P., Müller, W., Nita, D.C., Ontañón, R., García-Moncó, C., Richards, D.A., 2019. North Iberian temperature and rainfall seasonality over the younger dryas and Holocene. *Quat. Sci. Rev.* 226, 105998.
- Bard, E., Delaygue, G., Rostek, F., Antonioli, F., Silenzi, S., Schrag, D.P., 2002. Hydrological conditions over the western Mediterranean basin during the deposition of the cold Sapropel 6 (ca. 175 kyr BP). *Earth Planet Sci. Lett.* 202, 481–494.
- Bar-Matthews, M., Ayalon, A., Matthews, A., Sass, E., Halicz, L., 1996. Carbon and oxygen isotope study of the active water-carbonate system in a karstic Mediterranean cave: implications for paleoclimate research in semiarid regions. *Geochem. Cosmochim. Acta* 60, 337–347.
- Bar-Matthews, M., Ayalon, A., Gilmour, M., Matthews, A., Hawkesworth, C.J., 2003. Sea–land oxygen isotopic relationships from planktonic foraminifera and speleothems in the Eastern Mediterranean region and their implication for paleorainfall during interglacial intervals. *Geochem. Cosmochim. Acta* 67, 3181–3199.
- Bar-Matthews, M., Ayalon, A., 2011. Mid-Holocene climate variations revealed by high-resolution speleothem records from Soreq Cave, Israel and their correlation with cultural changes. *Holocene* 21, 163–171.
- Batchelor, C.L., Margold, M., Krapp, M., Murton, D.K., Dalton, A.S., Gibbard, P.L., Stokes, C.R., Murton, J.B., Manica, A., 2019. The configuration of Northern Hemisphere ice sheets through the Quaternary. *Nat. Commun.* 10, 1–10.
- Beck, H.E., Zimmermann, N.E., McVicar, T.R., Vergopolan, N., Berg, A., Wood, E.F., 2018. Present and future Köppen-geiger climate classification maps at 1-km resolution. *Sci. Rep.* 5, 180214.
- Berger, A.L., 1978. Long-term variations of caloric insolation resulting from the earth's orbital elements. *Quat. Res.* 9, 139–167.
- Boch, R., Cheng, H., Spötl, C., Edwards, R.L., Wang, X., Häuselmann, P., 2011. NALPS: a precisely dated European climate record 120–60 ka. *Clim. Past* 7, 1247–1259.
- Bond, G., Kromer, B., Beer, J., Muscheler, R., Evans, M.N., Showers, W., Hoffmann, S., Lotti-Bond, R., Hajdas, I., Bonani, G., 2001. Persistent solar influence on North Atlantic climate during the Holocene. *Science* 294, 2130–2136.
- Budsky, A., Wassenburg, J.A., Mertz-Kraus, R., Spötl, C., Jochum, K.P., Gibert, L., Scholz, D., 2019. Western Mediterranean climate response to Dansgaard/Oeschger events: new insights from speleothem records. *Geophys. Res. Lett.* 46, 9042–9053.
- Celle-Jeanton, H., Travi, Y., Blavoux, B., 2001. Isotopic typology of the precipitation in the Western Mediterranean region at the three different time scales. *Geophys. Res. Lett.* 28, 1215–1218.
- Channell, J.E.T., Hodell, D.A., Romero, O., Hillaire-Marcel, C., de Vernal, A., Stoner, J.S., Mazaud, A., Röhl, U., 2012. A 750-kyr detrital-layer stratigraphy for the north Atlantic (IODP sites U1302–U1303, orphan Knoll, Labrador sea). *Earth Planet Sci.*

- Lett. 317–318, 218–230.
- Chapman, M.R., Shackleton, N.J., 1999. Global ice-volume fluctuations, North Atlantic ice-raftering events, and deep-ocean circulation changes between 130 and 70 ka. *Geology* 27, 795–798.
- Cheng, H., Edwards, R.L., Shen, C.-C., Polyak, V.J., Asmerom, Y., Woodhead, J., Hellstrom, J., Wang, Y., Kong, X., Spötl, C., Wang, X., Alexander Jr., E.C., 2013. Improvements in  $^{230}\text{Th}$  dating,  $^{230}\text{Th}$  and  $^{234}\text{U}$  half-life values, and U-Th isotopic measurements by multi-collector inductively coupled plasma mass spectrometry. *Earth Planet Sci. Lett.* 371, 82–91.
- Cheng, H., Edwards, R.L., Sinha, A., Spötl, C., Yi, L., Chen, S., Kelly, M., Kathayat, G., Wang, X., Li, X., Kong, X., Wang, Y., Ning, Y., Zhang, H., 2016. The Asian monsoon over the past 640,000 years and ice age terminations. *Nature* 534, 640–646.
- Columbu, A., Sauro, F., Lundberg, J., Drysdale, R., de Waele, J., 2018. Palaeoenvironmental changes recorded by speleothems of the southern Alps (Piani Eterni, Belluno, Italy) during four interglacial to glacial climate transitions. *Quat. Sci. Rev.* 197, 319–335.
- Columbu, A., Spötl, C., De Waele, J., Yu, T.-L., Shen, C.-C., Gázquez, F., 2019. A long record of MIS 7 and MIS 5 climate and environment from a western Mediterranean speleothem (SW Sardinia, Italy). *Quat. Sci. Rev.* 220, 230–243.
- Columbu, A., Chiarini, V., Spötl, C., Benazzi, S., Hellstrom, J., Cheng, H., De Waele, J., 2020. Speleothem record attests to stable environmental conditions during Neanderthal–modern human turnover in southern Italy. *Nat. Ecol. Evol.* 4, 1188–1195.
- Dansgaard, W., Johnsen, S.J., Clausen, H.B., Dahl-Jensen, D., Gundestrup, N.S., Hammer, C.U., Hvidberg, C.S., Steffensen, J.P., Sveinbjörnsdóttir, A.E., Jouzel, J., Bond, G., 1993. Evidence for general instability of past climate from a 250-kyr ice-core record. *Nature* 364, 218–220.
- Day, C.C., Henderson, G.M., 2013. Controls on trace-element partitioning in cave-analogue calcite. *Geochem. Cosmochim. Acta* 120, 612–627.
- de Abreu, L., Shackleton, N.J., Schönfeld, J., Hall, M., Chapman, M., 2003. Millennial-scale oceanic climate variability off the Western Iberian margin during the last two glacial periods. *Mar. Geol.* 196, 1–20.
- Deininger, M., McDermott, F., Mudelsee, M., Werner, M., Frank, N., Mangini, A., 2017. Coherency of late Holocene European speleothem  $\delta^{18}\text{O}$  records linked to North Atlantic Ocean circulation. *Clim. Dynam.* 49, 595–618.
- Denniston, R.F., Houts, A.N., Asmerom, Y., Wanamaker, A.D., Haws, J.A., Polyak, V.J., Thatcher, D.L., Altan-Ochir, S., Borowski, A.C., Breitenbach, S.F.M., Ummenhofer, C.C., Regala, F.T., Benedetti, M.M., Bicho, N.F., 2018. A stalagmite test of North Atlantic SST and Iberian hydroclimate linkages over the last two glacial cycles. *Clim. Past* 14, 1893–1913.
- Dominguez-Villar, D., Wang, X., Krklec, K., Cheng, H., Edwards, R.L., 2017. The control of the tropical North Atlantic on Holocene millennial climate oscillations. *Geology* 45, 303–306.
- Dorale, J.A., Liu, Z., 2009. Limitations of hendy test criteria in judging the paleoclimatic suitability of speleothems and the need for replication. *J. Cave Karst Stud.* 71, 73–80.
- Drijfhout, S., Gleeson, E., Dijkstra, H.A., Livina, V., 2013. Spontaneous abrupt climate change due to an atmospheric blocking–sea-ice–ocean feedback in an unforced climate model simulation. *Proc. Natl Acad. Sci.* 110, 19713–19718.
- Drysdale, R.N., Zanchetta, G., Hellstrom, J.C., Fallick, A.E., Zhao, J.X., 2005. Stalagmite evidence for the onset of the Last Interglacial in southern Europe at  $129 \pm 1$  ka. *Geophys. Res. Lett.* 32, L24708.
- Drysdale, R.N., Hellstrom, J.C., Zanchetta, G., Fallick, A.E., Sánchez Goñi, M.F., Couchoud, I., McDonald, J., Maas, R., Lohmann, G., Isola, I., 2009. Evidence for obliquity forcing of glacial Termination II. *Science* 325, 1527–1531.
- Drysdale, R., Couchoud, I., Zanchetta, G., Isola, I., Regattieri, E., Hellstrom, J., Govin, A., Tzedakis, P.C., Ireland, T., Corrick, E., Greig, A., Wong, H., Piccini, L., Holden, P., Woodhead, J., 2020. Magnesium in subaqueous speleothems as a potential palaeotemperature proxy. *Nat. Commun.* 11, 1–11.
- Dumitru, O.A., Onac, B.P., Polyak, V.J., Wynn, J.G., Asmerom, Y., Fornós, J.J., 2018. Climate variability in the western Mediterranean between 121 and 67 ka derived from a Mallorcan speleothem record. *Palaeogeogr. Palaeoclimatol. Palaeoecol.* 506, 128–138.
- Fairchild, I.J., Borsato, A., Tooth, A.F., Frisia, S., Hawkesworth, C.J., Huang, Y., McDermott, F., Spiro, B., 2000. Controls on trace element (Sr–Mg) compositions of carbonate cave waters: implications for speleothem climatic records. *Chem. Geol.* 166, 255–269.
- Fairchild, I.J., Smith, C.L., Baker, A., Fuller, L., Spötl, C., Matthey, D., McDermott, F., 2006. Modification and preservation of environmental signals in speleothems. *Earth Sci. Rev.* 75, 105–153.
- Fohlmeister, J., 2012. A statistical approach to construct composite climate records of dated archives. *Quat. Geochronol.* 14, 48–56.
- Fohlmeister, J., Arps, J., Spötl, C., Schröder-Ritzrau, A., Plessen, B., Günter, C., Frank, N., Trüssel, M., 2018. Carbon and oxygen isotope fractionation in the water–calcite–aragonite system. *Geochem. Cosmochim. Acta* 235, 127–139.
- Friedrich, T., Timmermann, A., Menviel, L., Elison Timm, O., Mouchet, A., Roche, D.M., 2010. The mechanism behind internally generated centennial-to-millennial scale climate variability in an earth system model of intermediate complexity. *Geosci. Model Dev. (GMD)* 3, 377–389.
- Frisia, S., Borsato, A., Preto, N., McDermott, F., 2003. Late Holocene annual growth in three Alpine stalagmites records the influence of solar activity and the North Atlantic Oscillation on winter climate. *Earth Planet Sci. Lett.* 216, 411–424.
- García-Ruiz, J.M., López-Moreno, J.I., Vicente-Serrano, S.M., Lasanta-Martínez, T., Beguería, S., 2011. Mediterranean water resources in a global change scenario. *Earth Sci. Rev.* 105, 121–139.
- Gilli, E., 1999. Evidence of palaeoseismicity in a flowstone of the observatoire cave (Monaco). *Geodin. Acta* 12, 159–168.
- Goosse, H., Brovkin, V., Fichefet, T., Haarsma, R., Huybrechts, P., Jongma, J., Mouchet, A., Sclaten, F., Barriat, P.-Y., Campin, J.-M., Deleersnijder, E., Driesschaert, E., Goelzer, H., Janssens, I., Loutre, M.-F., Morales Maqueda, M.A., Opsteegh, T., Mathieu, P.-P., Munhoven, G., Pettersson, E.J., Renssen, H., Roche, D.M., Schaeffer, M., Tartini, B., Timmermann, A., Weber, S.L., 2010. Description of the earth system model of intermediate complexity LOVECLIM version 1.2. *Geosci. Model Dev. (GMD)* 3, 603–633.
- Grant, K.M., Rohling, E.J., Bar-Matthews, M., Ayalon, A., Medina-Elizalde, M., Ramsey, C.B., Satow, C., Roberts, A.P., 2012. Rapid coupling between ice volume and polar temperature over the past 150,000 years. *Nature* 491, 744–747.
- Hendy, C.H., 1971. The isotopic geochemistry of speleothems-I. The calculation of the effects of different modes of formation on the isotopic composition of speleothems and their applicability as palaeoclimatic indicators. *Geochem. Cosmochim. Acta* 35, 801–824.
- Heusser, L., Oppo, D.W., 2003. Millennial- and orbital-scale climate variability in southeastern United States and in the subtropical Atlantic during Marine Isotope Stage 5: evidence from pollen and isotopes in ODP Site 1059. *Earth Planet Sci. Lett.* 214, 483–490.
- Hoerling, M., Eischeid, J., Perlwitz, J., Quan, X., Zhang, T., Pegion, P., 2012. On the increased frequency of Mediterranean drought. *J. Clim.* 25, 2146–2161.
- Hu, H.-M., et al., 2022. Tracking westerly wind directions over Europe since the middle Holocene. *Science Advances*. Submitted for publication.
- Hurrell, J.W., 1995. Decadal trends in the North Atlantic oscillation: regional temperatures and precipitation. *Science* 269, 676–679.
- Ionita, M., Scholz, P., Lohmann, G., Dima, M., Prange, M., 2016. Linkages between atmospheric blocking, sea ice export through Fram Strait and the Atlantic meridional overturning circulation. *Sci. Rep.* 6, 1–10.
- Jackson, L.C., Kahana, R., Graham, T., Ringer, M.A., Woollings, T., Mecking, J.V., Wood, R.A., 2015. Global and European climate impacts of a slowdown of the AMOC in a high resolution GCM. *Clim. Dynam.* 45, 3299–3316.
- Johnsen, S.J., Clausen, H.B., Dansgaard, W., Fuhrer, K., Gundestrup, N., Hammer, C.U., Iversen, P., Jouzel, J., Stauffer, B., Steffensen, J.P., 1992. Irregular glacial interstadials recorded in a new Greenland ice core. *Nature* 359, 311–313.
- Kageyama, M., Merkel, U., Otto-Bliesner, B., Prange, M., Abe-Ouchi, A., Lohmann, G., Ohgaito, R., Roche, D.M., Singarayer, J., Swingedouw, D., Zhang, X., 2013. Climatic impacts of fresh water hosing under last glacial maximum conditions: a multi-model study. *Clim. Past* 9, 935–953.
- Kindler, P., Guillevic, M., Baumgartner, M., Schwander, J., Landais, A., Leuenberger, M., et al., 2014. Temperature reconstruction from 10 to 120 kyr b2k from the NGRIP ice core. *Climate of the Past* 10, 887–902. <https://doi.org/10.5194/cp-10-887-2014>.
- Kleppin, H., Jochum, M., Otto-Bliesner, B., Shields, C.A., Yeager, S., 2015. Stochastic atmospheric forcing as a cause of Greenland climate transitions. *J. Clim.* 28, 7741–7763.
- Kodera, K., 2002. Solar cycle modulation of the north Atlantic oscillation: implication in the spatial structure of the NAO. *Geophys. Res. Lett.* 29, 59-1.
- Köhler, P., Nehrass-Ahles, C., Schmitt, J., Stocker, T.F., Fischer, H., 2017. A 156 kyr smoothed history of the atmospheric greenhouse gases CO<sub>2</sub>, CH<sub>4</sub>, and N<sub>2</sub>O and their radiative forcing. *Earth Syst. Sci. Data* 9, 363–387.
- Lachniet, M.S., 2009. Climatic and environmental controls on speleothem oxygen-isotope values. *Quat. Sci. Rev.* 28, 412–432.
- Lambeck, K., Chappell, J., 2001. Sea level change through the last glacial cycle. *Science* 292, 679–686.
- Laskar, J., Fienga, A., Gastineau, M., Manche, H., 2011. La2010: a new orbital solution for the long-term motion of the Earth. *Astron. Astrophys.* 532, A89.
- Lisiecki, L.E., Raymo, M.E., 2005. A Pliocene-Pleistocene stack of 57 globally distributed benthic  $\delta^{18}\text{O}$  records. *Paleoceanography* 20, PA1003.
- Ludwig, P., Schaffernicht, E.J., Shao, Y., Pinto, J.G., 2016. Regional atmospheric circulation over Europe during the last glacial maximum and its links to precipitation. *J. Geophys. Res.* 121, 2130–2145.
- Luetscher, M., Boch, R., Sodemann, H., Spötl, C., Cheng, H., Edwards, R.L., Frisia, S., Hof, F., Müller, W., 2015. North Atlantic storm track changes during the last glacial maximum recorded by Alpine speleothems. *Nat. Commun.* 6, 6344.
- Mangini, A., Spötl, C., Verdes, P., 2005. Reconstruction of temperature in the central Alps during the past 2000 yr from a  $\delta^{18}\text{O}$  stalagmite record. *Earth Planet Sci. Lett.* 235, 741–751.
- Margari, V., Skinner, L.C., Tzedakis, P.C., Ganopolski, A., Vautravers, M., Shackleton, N.J., 2010. The nature of millennial-scale climate variability during the past two glacial periods. *Nat. Geosci.* 3, 127–131.
- Martrat, B., Grimalt, J.O., Lopez-Martinez, C., Cacho, I., Sierro, F.J., Flores, J.A., Zahn, R., Canals, M., Curtis, J.H., Hodell, D.A., 2004. Abrupt temperature changes in the Western Mediterranean over the past 250,000 years. *Science* 306, 1762–1765.
- Merz, N., Raible, C.C., Woollings, T., 2015. North Atlantic eddy-driven jet in interglacial and glacial winter climates. *J. Clim.* 28, 3977–3997.
- McDermott, F., 2004. Palaeo-climate reconstruction from stable isotope variations in speleothems: a review. *Quat. Sci. Rev.* 23, 901–918.
- Milner, A.M., Müller, U.C., Roucoux, K.H., Collier, R.E., Pross, J., Kalaitzidis, S., Christakis, K., Tzedakis, P.C., 2013. Environmental variability during the last interglacial: a new high-resolution pollen record from Tenaghi Philippon, Greece. *J. Quat. Sci.* 28, 113–117.
- Mokeddem, Z., McManus, J.F., 2016. Persistent climatic and oceanographic oscillations in the subpolar North Atlantic during the MIS 6 glaciation and MIS 5

- interglacial. *Paleoceanography* 31, 758–778.
- Morley, A., Rosenthal, Y., DeMenocal, P., 2014. Ocean-atmosphere climate shift during the mid-to-late Holocene transition. *Earth Planet Sci. Lett.* 388, 18–26.
- Naumann, G., Cammalleri, C., Mentaschi, L., Feyen, L., 2021. Increased economic drought impacts in Europe with anthropogenic warming. *Nat. Clim. Change* 11, 485–491.
- NorthGRIP-Members, 2004. High-resolution record of Northern Hemisphere climate extending into the last interglacial period. *Nature* 431, 147–151.
- O'Neil, J.R., Clayton, R.N., Mayeda, T.K., 1969. Oxygen isotope fractionation in divalent metal carbonates. *J. Chem. Phys.* 51, 5547–5558.
- Oppo, D.W., Horowitz, M., Lehman, S.J., 1997. Marine core evidence for reduced deep water production during Termination II followed by a relatively stable substage 5e (Eemian). *Paleoceanography* 12, 51–63.
- Regattieri, E., Zanchetta, G., Isola, I., Zanella, E., Drysdale, R.N., Hellstrom, J.C., Zerbini, A., Dallai, L., Tema, E., Lanci, L., Costa, E., Magri, F., 2019. Holocene critical zone dynamics in an Alpine catchment inferred from a speleothem multiproxy record: disentangling climate and human influences. *Sci. Rep.* 9, 1–9.
- Risebrobakken, B., Dokken, T., Jansen, E., 2005. Extent and variability of the meridional Atlantic circulation in the eastern Nordic seas during marine isotope stage 5 and its influence on the inception of the last glacial. *Geophys. Monogr.* 158, 323–339.
- Rohling, E.J., Marino, G., Grant, K.M., 2015. Mediterranean climate and oceanography, and the periodic development of anoxic events (sapropels). *Earth Sci. Rev.* 143, 62–97.
- Romanek, C.S., Grossman, E.L., Morse, J.W., 1992. Carbon isotopic fractionation in synthetic aragonite and calcite: effects of temperature and precipitation rate. *Geochem. Cosmochim. Acta* 56, 419–430.
- Rossoni-Notter, E., Notter, O., Simone, S., Simon, P., 2016. Acheulean in Monaco: observatoire cave and its singular occupations. *Quat. Int.* 411, 212–235.
- Ruan, J., Kherbouche, F., Genty, D., Blamart, D., Cheng, H., Dewilde, F., Hachi, S., Edwards, R.L., Régnier, E., Michelot, J.L., 2016. Evidence of a prolonged drought ca. 4200 yr BP correlated with prehistoric settlement abandonment from the Gueldaman GLD1 Cave, Northern Algeria. *Clim. Past* 12, 1–14.
- Sánchez Goñi, M.F., Eynaud, F., Turon, J.L., Shackleton, N.J., 1999. High resolution palynological record off the Iberian margin: direct land-sea correlation for the last interglacial complex. *Earth Planet Sci. Lett.* 171, 123–137.
- Scholz, D., Hoffmann, D.L., 2011. StalAge - an algorithm designed for construction of speleothem age models. *Quat. Geochronol.* 6, 369–382.
- Scholz, D., Frisia, S., Borsato, A., Spötl, C., Fohlmeister, J., Mudelsee, M., Miorandi, R., Mangini, A., 2012. Holocene climate variability in north-eastern Italy: potential influence of the NAO and solar activity recorded by speleothem data. *Clim. Past* 8, 1367–1383.
- Schulz, M., Mudelsee, M., 2002. REDFIT: estimating red-noise spectra directly from unevenly spaced paleoclimatic time series. *Comput. Geosci.* 28, 421–426.
- Shen, C.-C., Cheng, H., Edwards, R.L., Moran, S.B., Edmonds, H.N., Hoff, J.A., Thomas, R.B., 2003. Measurement of attogram quantities of  $^{231}\text{Pa}$  in dissolved and particulate fractions of seawater by isotope dilution thermal ionization mass spectroscopy. *Anal. Chem.* 75, 1075–1079.
- Shen, C.-C., Li, K.-S., Sieh, K., Natawidjaja, D., Cheng, H., Wang, X., Edwards, R.L., Lam, D.D., Hsieh, Y.-Te, Fan, T.-Y., Meltzner, A.J., Taylor, F.W., Quinn, T.M., Chiang, H.-W., Kilbourne, K.H., 2008. Variation of initial  $^{230}\text{Th}/^{232}\text{Th}$  and limits of high precision U-Th dating of shallow-water corals. *Geochem. Cosmochim. Acta* 72, 4201–4223.
- Shen, C.-C., Wu, C.-C., Cheng, H., Edwards, R.L., Hsieh, Y.-Te, Gallet, S., Chang, C.-C., Li, T.-Y., Lam, D.D., Kano, A., Hori, M., Spötl, C., 2012. High-precision and high-resolution carbonate  $^{230}\text{Th}$  dating by MC-ICP-MS with SEM protocols. *Geochem. Cosmochim. Acta* 99, 71–86.
- Smeed, D.A., Josey, S.A., Beaulieu, C., Johns, W.E., Moat, B.I., Frajka-Williams, E., Rayner, D., Meinen, C.S., Baringer, M.O., Bryden, H.L., McCarthy, G.D., 2018. The North Atlantic Ocean is in a state of reduced overturning. *Geophys. Res. Lett.* 45, 1527–1533.
- Smith, A.C., Wynn, P.M., Barker, P.A., Leng, M.J., Noble, S.R., Tych, W., 2016. North Atlantic forcing of moisture delivery to Europe throughout the Holocene. *Sci. Rep.* 6, 1–7.
- Spratt, R.M., Lisiecki, L.E., 2016. A late Pleistocene sea level stack. *Clim. Past* 12, 1079–1092.
- Sprovieri, R., Di Stefano, E., Incarbona, A., Oppo, D.W., 2006. Suborbital climate variability during Marine Isotopic Stage 5 in the central Mediterranean basin: evidence from calcareous plankton record. *Quat. Sci. Rev.* 25, 2332–2342.
- Stockhecke, M., Timmermann, A., Kipfer, R., Haug, G.H., Kwiceniec, O., Friedrich, T., Menviel, L., Litt, T., Pickarski, N., Anselmetti, F.S., 2016. Millennial to orbital-scale variations of drought intensity in the Eastern Mediterranean. *Quat. Sci. Rev.* 133, 77–95.
- Stouffer, R.J., Yin, J., Gregory, J.M., Dixon, K.W., Spelman, M.J., Hurlin, W., Weaver, A.J., Eby, M., Flato, G.M., Hasumi, H., Hu, A., Jungclaus, J.H., Kamenkovich, I.V., Levermann, A., Montoya, M., Murakami, S., Nawrath, S., Oka, A., Peltier, W.R., Robitaille, D.Y., Sokolov, A., Vettoretti, G., Weber, S.L., 2006. Investigating the causes of the response of the thermohaline circulation to past and future climate changes. *J. Clim.* 19, 1365–1387.
- Suess, H.E., 1980. The radiocarbon record in tree rings of the last 8000 years. *Radiocarbon* 22, 200–209.
- Thatcher, D.L., Wanamaker, A.D., Denniston, R.F., Ummenhofer, C.C., Regala, F.T., Jorge, N., Haws, J., Chormann, A., Gillikin, D.P., 2020a. Linking the karst record to atmospheric, precipitation, and vegetation dynamics in Portugal. *Chem. Geol.* 558, 119949.
- Thatcher, D.L., Wanamaker, A.D., Denniston, R.F., Asmerom, Y., Polyak, V.J., Fullick, D., Ummenhofer, C.C., Gillikin, D.P., Haws, J.A., 2020b. Hydroclimate variability from western Iberia (Portugal) during the Holocene: insights from a composite stalagmite isotope record. *Holocene* 30, 966–981.
- Thiéblemont, R., Matthes, K., Omrani, N.E., Kodera, K., Hansen, F., 2015. Solar forcing synchronizes decadal North Atlantic climate variability. *Nat. Commun.* 6, 1–8.
- Tzedakis, P.C., Frogley, M.R., Heaton, T.H.E., 2003. Last Interglacial conditions in southern Europe: evidence from Ioannina, northwest Greece. *Global Planet. Change* 36, 157–170.
- Tzedakis, P.C., Drysdale, R.N., Margari, V., Skinner, L.C., Menviel, L., Rhodes, R.H., Taschetto, A.S., Hodell, D.A., Crowhurst, S.J., Hellstrom, J.C., Fallick, A.E., Grimalt, J.O., McManus, J.F., Martrat, B., Mokeddem, Z., Parrenin, F., Regattieri, E., Roe, K., Zanchetta, G., 2018. Enhanced climate instability in the North Atlantic and southern Europe during the last interglacial. *Nat. Commun.* 9, 1–14.
- Vanghi, V., Borsato, A., Frisia, S., Drysdale, R., Hellstrom, J., Bajo, P., 2018. Climate variability on the Adriatic seaboard during the last glacial inception and MIS 5c from Frassati Cave stalagmite record. *Quat. Sci. Rev.* 201, 349–361.
- Wassenburg, J.A., Dietrich, S., Fietzke, J., Fohlmeister, J., Jochum, K.P., Scholz, D., Richter, D.K., Sabaoui, A., Spötl, C., Lohmann, G., Andreae, M.O., Immenhauser, A., 2016. Reorganization of the north Atlantic oscillation during early Holocene deglaciation. *Nat. Geosci.* 9, 6–11.
- Wolff, E.W., Chappellaz, J., Blunier, T., Rasmussen, S.O., Svensson, A., 2010. Millennial-scale variability during the last glacial: the ice core record. *Quat. Sci. Rev.* 29, 2828–2838.
- Yin, Q.Z., Wu, Z.P., Berger, A., Gooze, H., Hodell, D., 2021. Insolation triggered abrupt weakening of Atlantic circulation at the end of interglacials. *Science* 373, 1035–1040.
- Yukimoto, S., Kodera, K., Thiéblemont, R., 2017. Delayed North Atlantic response to solar forcing of the stratospheric polar vortex. *SOLA* 13, 53–58.
- Zhou, J., Lundstrom, C.C., Fouke, B., Panno, S., Hackley, K., Curry, B., 2005. Geochemistry of speleothem records from southern Illinois: development of  $(^{234}\text{U})/(^{238}\text{U})$  as a proxy for paleoprecipitation. *Chem. Geol.* 22, 1–20.